Semiconductor Physics, Quantum Electronics & Optoelectronics, 2026. V. 29, No 2. P. 228-238.

Optoelectronics and optoelectronic devices

Plane-focusing optics for silicon solar photoconverters

E.E. Antonov[1*], V.V. Chernenko[2], V.P. Kostylyov[2*], V.S. Lysenko[2], D.Yu. Manko[1], I.A. Martynyuk[1], V.V. Petrov[1], V.N. Zenin[1]

[1]*Institute for Information Recording, National Academy of Sciences of Ukraine, 2 Shpak Street, 03113 Kyiv, Ukraine*
[2]*V. Lashkaryov Institute of Semiconductor Physics, National Academy of Sciences of Ukraine, 41 Nauky Avenue, 03028 Kyiv, Ukraine*
[*]*Corresponding author e-mail: antv1947@gmail.com; vkostylyov@ukr.net*

Abstract. A simulation algorithm has been developed and geometric parameters of plane-focusing lenses for concentrator solar energy systems with Si photoconverters have been calculated. These lenses form a homogeneous image in the focal plane, so they are promising for use in such systems and allow minimizing thermal and electrical losses in solar modules caused by non-uniform illumination of the photoconverter surface. A technology of manufacturing stamp-matrixes by diamond microcutting has been developed. Based on the simulation results, a number of plane-focusing lens samples have been formed by thermopressing technique using metal matrices. The manufactured samples of square-shaped specialized transforming microprismatic structures have been experimentally investigated using a collimated laser beam.

Keywords: microprism simulation algorithm, plane-focusing optics, microrelief structure.

https://doi.org/10.15407/spqeo29.02.228
PACS 07.60.-j, 42.79.-e, 85.60.-q

Manuscript received 14.10.25; revised version received 17.03.26; accepted for publication 10.06.26; published online 23.06.26.

1. Introduction

In recent years, plane-focusing optics is becoming increasingly widespread [1–11]. Such optics forms a uniformly illuminated light spot in their focus for a parallel incident light beam. This phenomenon is the opposite to the one for traditional Fresnel lenses, which form a point image in their focus. The dependence of the focal intensity for traditional lenses $J(r)$ on the image radius r is $J(r) \sim 1/r$. The Institute for Information Recording of the National Academy of Sciences of Ukraine (IIR Ukraine) is also actively working on creating the plane-focusing optics [12, 13]. The areas of its application are quite diverse: from automated control systems for moving objects to concentrator modules for solar energy systems, and from precision surface treatment of metals and plastics to laser photolithography. In IIR Ukraine, an algorithm for simulating the parameters of plane-focusing lenses has been developed, a technology for forming matrices and replicating final products has been proposed, and prototypes of microprism transforming Fresnel lenses have been manufactured.

The created algorithm for simulating flat-focusing lenses is described in detail in our previous papers [12, 13]. It allows one to create plane-focusing lenses from an optical material with refractive index n_0 for different diameters of the light beam D_L and with required focal length f_0. Depending on the purpose, such lenses should form homogeneous light circles of different radii r_V in the lens focus.

In this work, we consider in more detail creation of flat-focusing optics for concentrator modules of solar energy systems. In this case, creation of a homogeneously illuminated circle on the photo-converter surface allows one to completely eliminate lateral currents [14–16], which have negative effect on the thermal balance and energy efficiency [17] of the module.

2. Algorithm for calculating the parameters of plane-focusing lenses

The algorithm for simulating the parameters of transforming microprism flat optics [13] first of all determines the lens illumination scheme (SL), *i.e.* the necessary distribution of the illumination in the focus – a light circle or a circle with a light ring on the periphery. In the center of this image, anon-illuminated "dark" area with a radius r_j (j = 0, 1, …, N) is simulated, which is created to eliminate the central intensity maximum and to homogenize the illumination. It is assumed [12] that this "dark" area is illuminated in practice with the light scattered by the defects of the lens microrelief.

At first stage of calculating the geometric parameters of the lenses, the required outer radius of the focal image r_V is set. Then the focusing process (OF) is optimized so that the corresponding refractive zones with a radius R_k and a width ΔR_k (k = 20…35) of the lens with a light beam diameter D_L should direct the refracted light beams into certain annular image regions with a width $\Delta r_j = r_V - r_j$.

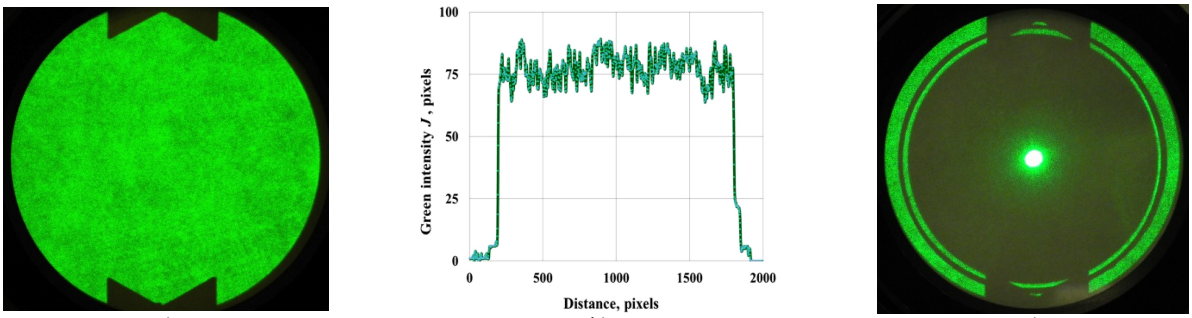

a) b) c)

Fig. 1. Image of a collimated laser beam on the screen (a), profile of this image (b), and the image of a transformed laser beam for the lens #31m-#04 (c).

For example, the scheme OF = 1.0(3)–2.0(1)–3.0(1) means that the first three zones of the lens, # 1–3, direct light into the image region with an inner radius $r_j = 1.0$ mm, the zone # 4 directs light into the region with a radius $r_j = 2.0$ mm, and the last zone # 5 – into the region with a radius $r_j = 3.0$ mm. The r_V can be of any value provided $D_L > r_V > r_j$.

To use the diamond microcutting technique [18–20] for manufacturing microprism optics, the refractive zones of the lens of a width ΔR_k can be created from several separate microprismatic components with a width ΔR_{kc}, identical in relief depth h_k and refractive angle α_k, *i.e.* $\Delta R_k = \Sigma\, \Delta R_{kc}$. The value of ΔR_{kc} cannot exceed 1.2…1.5 mm [19, 20], which corresponds to the dimensions of the cutting edge of the existing diamond tool.

The calculations also take into account the narrowing of light fluxes by applying appropriate correction of the width of the prismatic lens zones ΔR_k [13]. However, such correction is necessary only for the zones consisting of one microprism. For the refractive zones created from several microprismatic components ΔR_{kc}, correction of the width of the zone ΔR_k is not required.

According to the algorithm presented above, corresponding metal stamp-matrices for lens replication were formed [12, 13] and a number of test lenses were made from polycarbonate blanks applying individual diamond microcutting technique.

3. Results of experimental study of the lenses

For experimental study of the manufactured samples of plane-focusing lenses, a special experimental set-up [13] was created, which allows obtaining an image of a parallel beam of laser light passing through the test lens on a matte translucent screen. The laser beam is created by a condenser system of three lenses. The wavelength of "green" laser $\lambda = 0.532$ μm and the diameter of the collimated light beam in the screen plane $D_S = 59$ mm.

The images of the transformed laser beam on the screen were recorded by a Nikon P7000 camera. Fixed focus settings and shooting parameters were used to allow direct comparison of the obtained intensities of screen illumination for different lenses. Fig. 1a shows a typical image of a collimated laser beam on the screen in the absence of lenses. Fig. 1b illustrates a profilogram of this image. Fig. 1c shows an image of a transmitted beam on the screen after its transformation by the "solar" lens #31m-#04 (the focal length $f_0 = 40$ mm for the wavelength $\lambda_0 = 0.585$ μm, the calculated radius of the light spot $r_V = 1.5$ mm, the radius of the "dark" area in the center of the image $r_j = 0.3$ mm, and the observation distance $L_0 = 40$ mm). In Fig. 1c, the central light spot of diameter d_S corresponds to the calculated value $d_V = 3.0$ mm.

The profile of the light intensity distribution in the focal plane was obtained using Jmage J-1.53 software [21]. The relationship between the geometric dimensions of the light spot d_S on the screen and its dimensions d_J at the Jmage J-profile is easy to determine knowing that the outer circle in Fig. 1a corresponds to the diameter of the collimated laser beam at the screen $d_S = 59$ mm. When the scanning scale is changed, the image size in pixels also changes. However, for the light intensity registration mode shown in Fig. 1, the image diameter at the Jmage J-1.53 screen $d_J = 1155$ pixels, *i.e.* a distance of 1.0 mm to the image on the screen corresponds to 19.57 pixels at the profile and, hence, the diameter $d_S = 3.0$ mm for the lens #31m-#04 on the screen is ~59 pixels.

The first samples of the so-called "solar" plane-focusing lenses for concentrator modules of solar energy systems [13] (the lenses #25c, #27, and #28) were simulated according to the "circle" SL illumination scheme for the wavelength $\lambda = 0.585$ μm and the refractive index $n_0 = 1.585$ according to the data [22]. The lenses were created with a light spot diameter $d_V = 3.0$ mm and a focal length $f_0 = 25$ mm to achieve a certain degree of solar rays concentration k_C. With a light lens diameter $D_L = 50$ mm, such lenses give the value $k_C \approx 280$. A sufficiently small value $f_0 = 25$ mm allows one to significantly reduce the thickness of the concentrator module, which can be created with such lenses. The size of the dark area r_j in the center of the focal image for these lenses was $r_j = 0.5$, 0.7 and 0.9 mm, respectively, to select the optimal design of the prism zones in our further developments.

Individually manufactured by the diamond microcutting technique, the "solar" lenses #25c, #27 and #28 were experimentally investigated at the modernized set-up [13] using a collimated "green" laser beam. Fig. 2 shows profilegrams of the transformed image for the lens #25c with a radius $r_j = 0.5$ mm and a focusing optimization

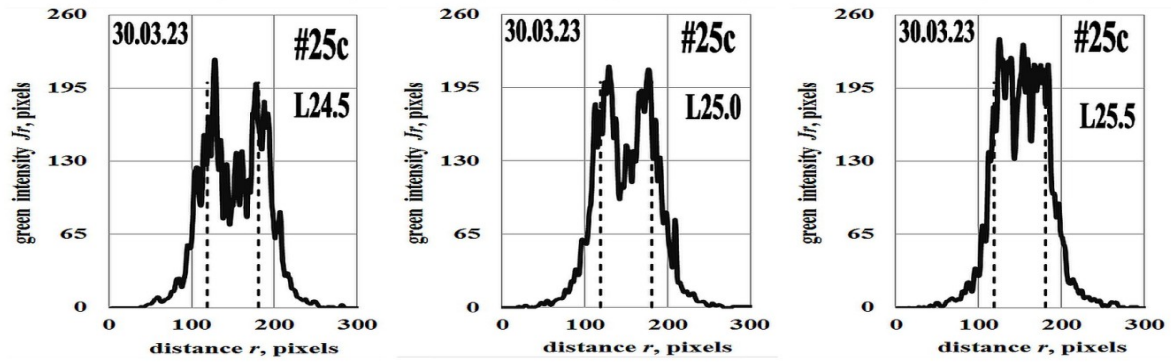

a) b) c)

Fig. 2. Spot profiles for the lens #25c and the observation distance L_0: a) 24.5, b) 25.0, and c) 25.5 mm.

scheme OF = 0.5(14)–0.8(2)–1.1(2). The calculated value of the light spot diameter $d_V = 3.0$ mm is shown in Fig. 2 by dashed lines.In the center of the light spot, for the nominal value $L_0 = 25$ mm, a certain decrease in the illumination level is observed. Therefore, even the value $r_j = 0.5$ mm for the radius of the "dark" area used in the calculations is too large to obtain a completely homogeneous illumination distribution. Hence, use of smaller values $r_j =$ 0.2…0.3 mm is advisable when creating such lenses in future.

The obtained data indicate that the shape of the profile noticeably changes even at small changes in the observation distance L_0. Hence, the shallow depth of focus for "solar" lenses with a focal length $f_0 = 25$ mm may be a problem during installing and focusing an array of individual lenses on a single platform when creating a solar module. For this reason, it is more practical to create "solar" lenses with a larger focal length $f_0 = 40…50$ mm. For such values of f_0, the depth of focus increases significantly [13], which simplifies the process

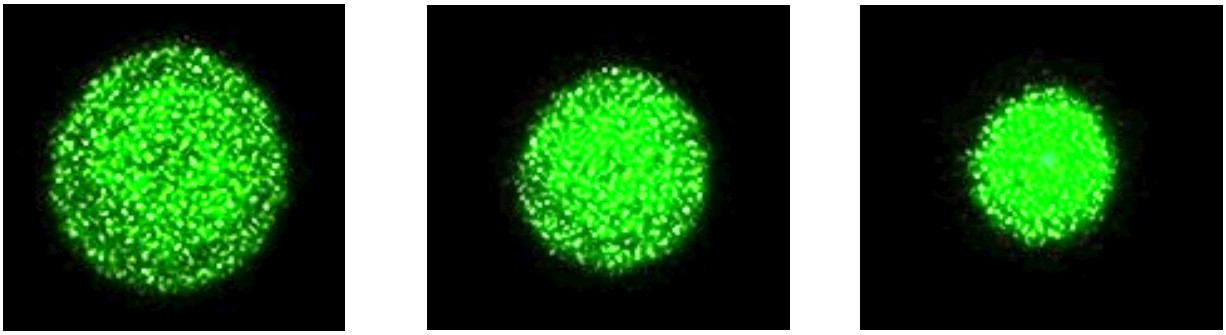

a) b) c)

Fig. 3. Focal images for the lens #31-#04 with focus $f = 40$ mm and radius $r_V = 1.5$ mm for the observation distance L_0: a) 39, b) 40, and c) 41 mm.

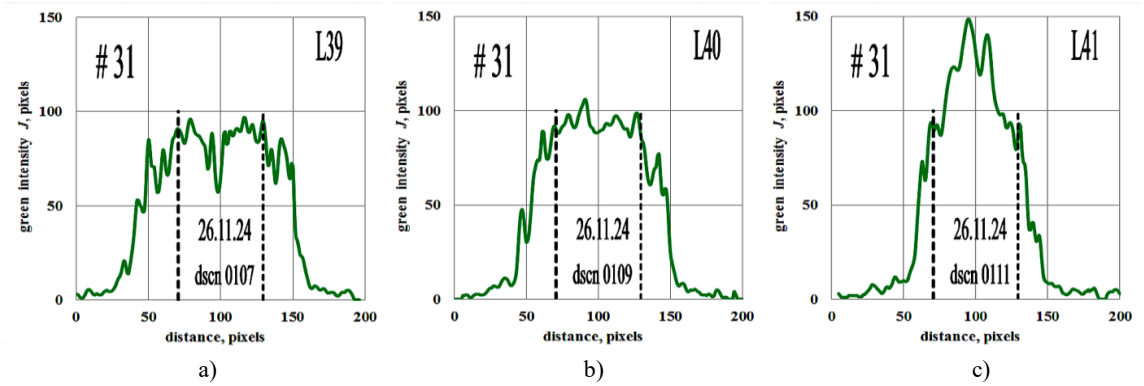

a) b) c)

Fig. 4. Profiles of focal images for the lens #31-#04 with focus $f = 40$ mm and radius $r_V = 1.5$ mm for the observation distance L_0: a) 39, b) 40, and c) 41 mm.

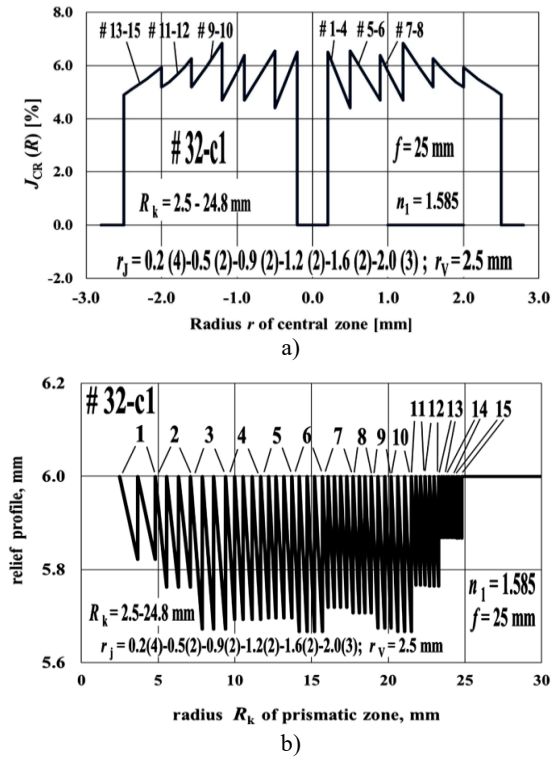

Fig. 5. Scheme of focusing optimization FO for the lens #32-c1 (a) and its relief structure (b).

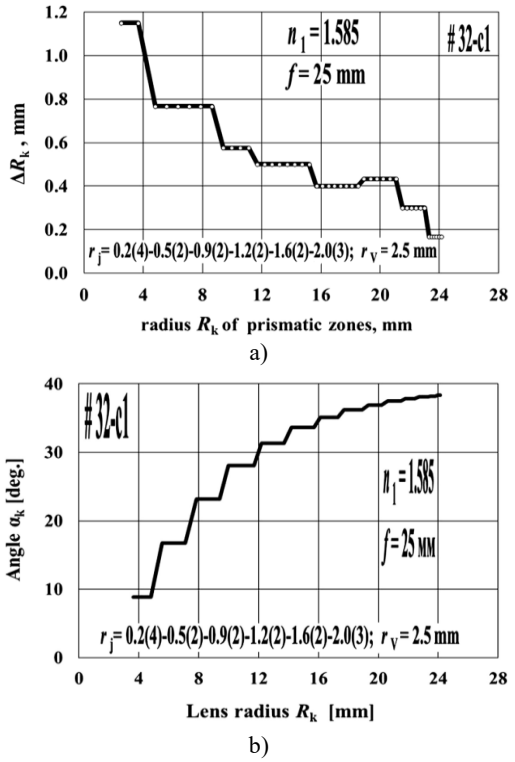

Fig. 6. Microrelief pitch ΔR_k for the lens #32-c1 (a) and refraction angle α_k (b).

of adjusting a large array of lenses (100–500) when creating industrial solar concentrator modules.

Therefore, the lens #31 was created with the radius $r_j = 0.3$ mm and the focal length $f_0 = 40$ mm. The lens-original #31orig and the stamp-matrix of this lens #31m were formed using the diamond microcutting technique [19, 20]. The reverse angle of the microprisms was set to $\theta = 3$ deg. to facilitate separating the metal matrix and the final plastic products during the thermopressing process [12]. A series of the lenses #31m-#(2-9) were manufactured using this process. The intensity distribution on the screen for the manufactured lens #31m-#04 obtained with the laser beam is shown in Fig. 3. The profilograms of these images for the observation distances $L_0 = 39$, 40 and 41 mm are presented in Fig. 4.

The obtained image profiles for the lens #31 are expanded compared to the calculated data (dashed line) similar to the lenses #25c, #27, and #28. The possible reason is the large contribution of light scattering on microrelief defects [13], because the radius $r_V = 1.5$ mm is quite small. Therefore, to diminish the contribution of scattering, we calculated the parameters of the lenses #32 and #32-c1, which form a larger focal image with $r_V = 2.5$ mm.

For further experimental studies, solar cells with combined diffusion-field barriers based on monocrystalline silicon [23, 24] are planned to use. Such cells were developed at the V. Lashkaryov Institute of Semiconductor Physics of the National Academy of Sciences of Ukraine. They are optimized for operation in the solar energy concentration mode [25, 26] and have individual cell dimensions of 5.0×5.0 mm^2, similar to those of [27, 28]. When using silicon photoconverters, the optimal concentration value is $k_C \approx 50…60$ [23–26]. The lenses #25c, #27, #28 and #31 provide a sufficiently high light concentration degree $k_C \approx 280$, but the lens #32 provides $k_C = 100$ for a light beam diameter $D_L = 50$ mm. After diaphragming this lens to a square shape with the maximum possible size of 35×35 mm^2, the degree of light concentration is reduced to $k_C \approx 60$. The above-mentioned diaphragming is also necessary to reduce losses of the incident light flux during creating an array of lenses in a single solar module.

The lenses #32 and #32-c1 with a radius of the "dark" area $r_j = 0.2$ mm and a focal length $f_0 = 25$ mm were calculated. Calculations of the parameters of the lens #32-c1 were performed using the radiation focusing optimization scheme FO = 0.2(4)–0.5(2)–0.9(2)–1.2(2) –1.6(2)–2.0(3), *i.e.* the first four lens zones, # 1-4, direct the radiation into a light ring of $r_V - r_j = 2.5 - 0.2 = 2.3$ mm, the next zones # 5-6 direct the radiation into a ring of $r_V - r_j = 2.5 - 0.5 = 2.0$ mm, the zones # 7-8 direct radiation into a ring of $r_V - r_j = 2.5 - 0.9 = 1.6$ mm, the zones #9-10 direct radiation into a light ring with a width $r_V - r_j = 2.5 - 1.2 = 1.3$ mm, two zones # 11-12 direct radiation into a ring with a width $r_V - r_j = 2.5 - 1.6 = 0.9$ mm, and the last peripheral zones # 13-15 direct radiation into a ring with a width $r_V - r_j = 2.5 - 2.0 = 0.5$ mm.

The applied light optimization scheme for the lens #32-c1 is illustrated in Fig. 5a. The calculated relief structure of this lens with pointed 15 zones is shown in Fig. 5b. The calculation fragment for the lens #32-c1 for the reverse microprism angle $\theta = 0$ deg. is shown in Appendix A.

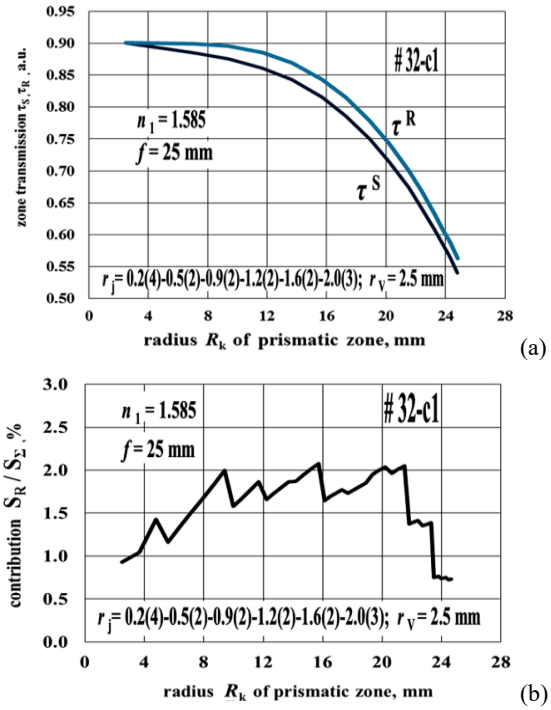

Fig. 7. Total light transmission coefficient of the lens #32-c1 (a) and contribution of each prismatic zone to the total light transmission (b).

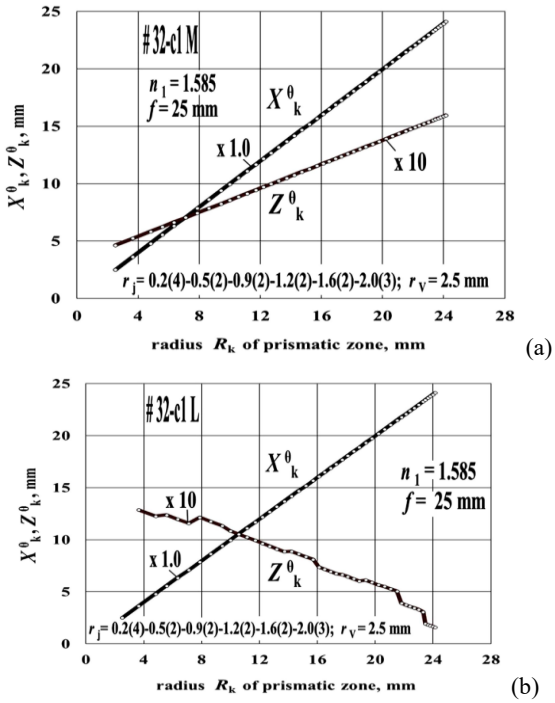

Fig. 8. Algorithm of moving the diamond cutter during manufacture of matrix #32-c1m (a) and the lens itself #32-c1L (b) for the microprism back angle θ = 3.0 deg.

The calculated microrelief pitch ΔR_k = 1150…167 μm (Fig. 6a) allows using an evaluable diamond cutter with a cutting edge length L_R = 1.8 mm for its formation. The maximum refraction angle of microprisms α_k = 38.4 deg. (Fig. 6b), which provides a sufficiently high light transmission τ_S.

The theoretical value of light transmission coefficient τ_S of the lens #32-c1 for its total optical aperture D_L = 49.6 mm is 74.97%. Light transmission by zones depending on the zone radius R_k is illustrated in Fig. 7a. The contribution of the individual lens zones to the total value of τ_S is 0.73–2.05%, which is illustrated in Fig. 7b. The coefficient τ_R describes Fresnel reflection. The value of τ_S also takes into account the so-called vignetting [12, 13] due to microprism back angle θ = 3.0 deg.

The algorithm of moving the diamond cutter when forming a metal stamp-matrix of the lens #32-c1m is illustrated in Fig. 8a. The matrix is formed with a microprism inclination angle θ = 3.0 deg., which ensures optimal separation of the matrix from the plastic final replicas during manufacturing final products by the thermopressing method. Fig. 8b illustrates the algorithm of moving the cutter when manufacturing originals of the lens #32-c1L directly by the individual diamond microcutting method with the same back angle of the microprisms θ = 3.0 deg.

The original lens #32-c1-orig and the stamp matrix of this lens #32-c1m with a back angle of the microprisms θ = 3 deg. were formed by the method of diamond microcutting. A series of the lenses #32m-#(1-12) was manufactured by the method of thermopressing with above matrix. The image of the stamp matrix #32c1m and the lens #32c1m-#5 of a square shape with the size 35×35 mm^2, made with this matrix, is shown in Fig. 9.

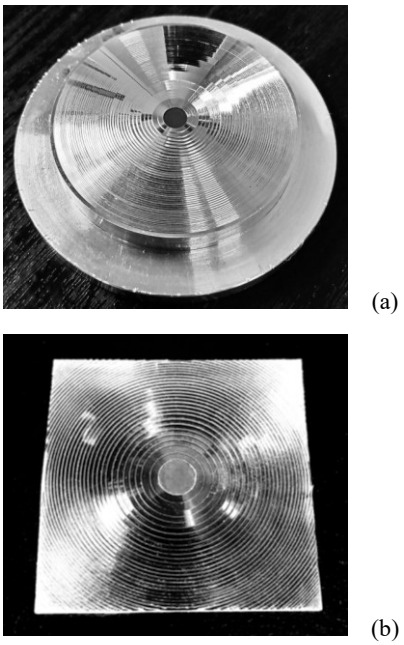

Fig. 9. General views of the stamp-matrix #32-c1m (a) and the square lens #32-c1m-#05 (b) with focus f = 25 mm and radius r_V = 2.5 mm.

The intensity distribution of a laser beam on the screen for the lens #32-c1m-#05 is shown in Fig. 10. The profilograms of these images are illustrated in Fig. 11 for the observation distances L_0 = 24, 25 and 26 mm. The width of the registered profiles practically coincides with their calculated values.

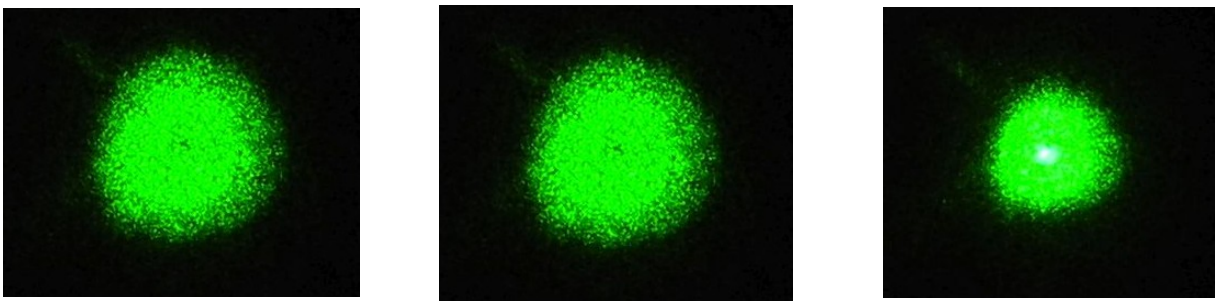

a) b) c)

Fig. 10. Focal images for the lens #32-c1m-#05 with focus $f = 25$ mm and radius $r_V = 2.5$ mm for the observation distance L_0: a) 24, b) 25, and c) 26 mm.

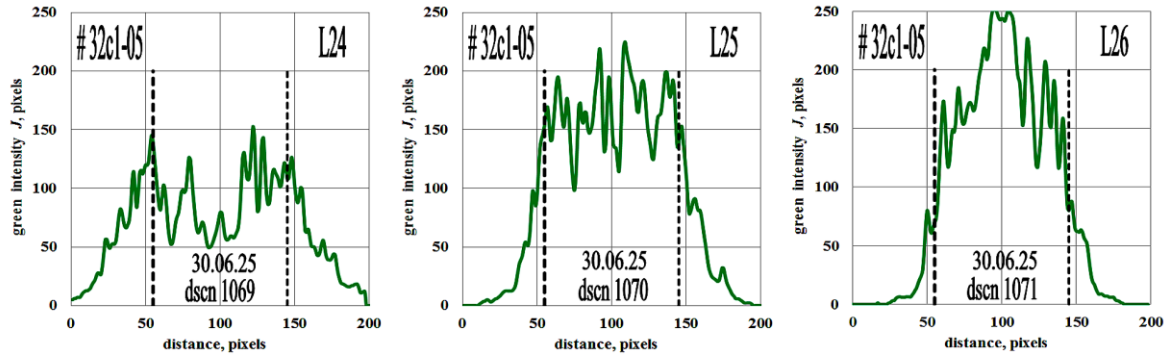

a) b) c)

Fig. 11. Profiles of focal images for the lens #32-c1m-#05 with focus $f = 25$ mm and radius $r_V = 2.5$ mm for the observation distance L_0: a) 24, b) 25, and c) 26 mm.

In our further studies of optical and thermal characteristics of "solar" lenses, photovoltaic cells made of crystalline silicon, for which the size of a unit cell of the available silicon plates is approximately 5.0×5.0 mm^2 similar to [27, 28], are planned to use. Therefore, when illuminating such a square cell with a circular light beam with a diameter $d_V = 2R_0$ (see Fig. 12a), two options are possible: (#1) a light circle with a diameter L_D is inscribed in a square with a radius R_{max} and (#2) a square with a radius R_{min} is inscribed in a circle with a diameter L_D. The flux diameter $d_V = 2R_{min}$ for the option #1. There are no flux losses (the area of the zone #1 = 0), but the area of the non-illuminated surface of the cell (zone #2 in Fig. 12a) is 27.32% of the total area of the light spot. For the option #2, the diameter $d_V = 2R_{max}$. The cell is illuminated completely (the area of the zone #2 = 0), but the light zone outside the working plane of the photoconverter (zone #1) is 41.42% of the flux area. The losses for the luminous flux (zone #1) and for the illumination area of the cell (zone #2) in the general case depending on the flux radius R_0 for the value of $L_D = 5.0$ mm are illustrated in Fig. 12b. In the optimal case, when the flux and illumination losses are the same and are about 9.0%, the optimal value $R_0/L_D = 1.12$. That is, for the cell measuring 5.0×5.0 mm^2, the optimal radius of a circular illumination flux is $R_0 = 2.82$ mm.

Hence, in the optimal variant, a silicon solar cell of the size 5.0×5.0 mm^2 should be illuminated with a circular light flux with a diameter $d_V \approx 5.7$ mm. The considered lenses #31 and #32-c1 totally satisfy the requirements of homogeneous illumination of a photoconverter surface. The size of the focal image L_D can be adjusted to the solar cell size by changing the observation distance L_0. For cells of the size 5.0×5.0 mm^2, to achieve the optimal size of the focal image of a round shape with a diameter $d_V \approx 5.7$ mm, the lens #31 should be used at the distance $L_0 \approx 38$ mm, and the lens #32-c1 should be placed at a distance $L_0 \approx$ 26 mm. However, a more optimal variant is to reshape the incident light flux to a square with the same size.

For use in a solar module, lenses with a diameter $D_L = 50$ mm should be apertured to a square shape with the maximum possible size of 35×35 mm^2. In this case, it is possible to compactly place an array of such lenses in a single module without losses of the incident light flux. An image of a diagnostic module consisting of four apertured lenses #32-c1-#(07-10) is shown in Fig. 13. Each of these lenses is made by thermopressing of blanks from optical polycarbonate with a thickness $Y = 2.0$ mm using a stamp-matrix made from W-95 alumina alloy. This matrix is formed by diamond microcutting technique according to the cutter movement algorithm shown in Fig. 8 with a modernized 6P82 machine tool [13].

The results of testing the optical characteristics of a single lens #32-c1-#05 ($D_L = 50$ mm, $f_0 = 25$ mm, and $r_V = 2.5$ mm), as well as a lens #31m-#06 ($D_L = 50$ mm, $f_0 = 40$ mm, and $r_V = 1.5$ mm), which are diaphragmed to a square shape measuring 35×35 mm^2, are shown in

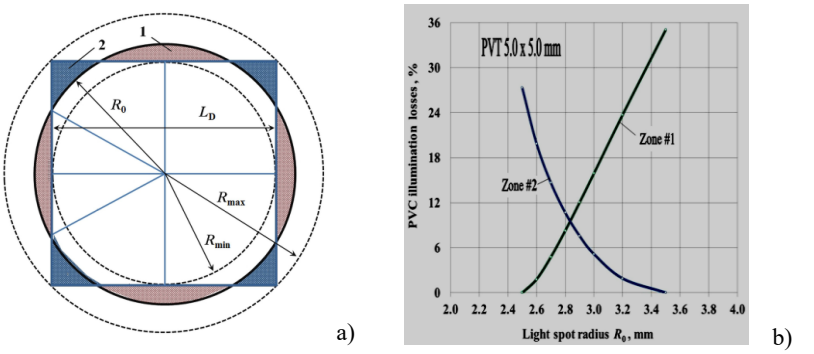

Fig. 12. Options for illumination of an $L_D \times L_D$ square cell by a circular light beam of a diameter $d_V = 2R_0$ (a) and relation of beam losses to illumination for a cell of the size 5.0×5.0 mm^2 (b).

Fig. 13. Image of a diagnostic module consisting of four apertured lenses #32-c1-#(07-10).

Fig. 14. These plane-focusing lenses were manufactured by thermopressing method using the corresponding metal stamp-matrices #32-c1m and #31m.

The obtained data show that varying the observation distance L_0, it is possible to obtain almost homogeneous square-shaped images sizing from the nominal value $L_S = 3.0$ mm (the lens #31m-#06) or $L_S = 5.0$ mm (the lens #32c1m-#05) to much larger sizes L_S, which can be almost equal to the dimensions of the lens itself. For example, the lens #31m-#06 creates homogeneous illumination of a square-shaped surface with a size $L_S = 5.0$ mm for an observation distance $L_0 \approx 39$ mm, and the lens #32c1m-#06 creates such illumination at a distance $L_0 \approx 27$ mm.

However, the detailed laser beam testing of the focusing properties of the lenses from the series #32c1m-#(01-12) revealed that the light spot in the focal plane of the lenses is somewhat expanded compared to the calculations, both for circular (Fig. 11) and square-shaped lenses (Fig. 14). Computer modeling using Solidwork 2016 and zones # 11-12 with the TracePro 7.3 softwares [29, 30] showed that the peripheral radii $R_k = 21.5$–23.3 mm of the lens-original #32-c1, and especially the refractive zones # 13-15 ($R_k = 23.3 \ldots 24.8$ mm) form additional refracted flows in the region outside the calculated focusing region due to reflection of the refracted rays inside the lens.

Fig. 15a shows profiles of the illumination distribution in the focal plane for the lens #32-c1 with a thickness $Y = 2.0$ mm for the total aperture ($R_k = 0 \ldots 24.8$ mm) as well as for individual groups of prism zones, which are formed according to the principle of uniformity of the radius r_j of the annular focusing areas with a width ($r_V - r_j$). The profiles are shown for an area radius $r_j = 0.2$ mm (the radii of the prism lens zones $R_k = 2.51 \ldots 1.7$ mm), $r_j = 0.5$ mm (the lens radii $R_k = 11.7 \ldots 15.7$ mm), $r_j = 0.9$ mm ($R_k = 15.7 \ldots 18.9$ mm), $r_j = 1.2$ mm ($R_k = 18.9 \ldots 21.5$ mm), $r_j = 1.6$ mm ($R_k = 21.5 \ldots 23.3$ mm), and a "dark" area radius $r_j = 2.0$ mm ($R_k = 23.3 \ldots 24.8$ mm).

Most of the prism zones direct the refracted rays into the calculated focusing area with $r_V = 2.5$ mm, which is shown in Fig. 15a by a dotted line. However, the lens zones # 11-15 form illuminated areas outside this focusing area. Fig. 15b shows the illumination distribution profile for the most problematic group of zones # 13-15 with the prism radii $R_k = 23.3 \ldots 24.8$ mm.

Appearance of an additional maximum at a radius $r_V = 4.3$ mm is explained by Fig. 16, which shows the simulated rays path through the prism zones # 13-15 of the lens #32-c1. The lens thickness is 2.0 mm, the flat translucent screen is placed at the distance of 25.0 mm, and the screen diameter is 50 mm.

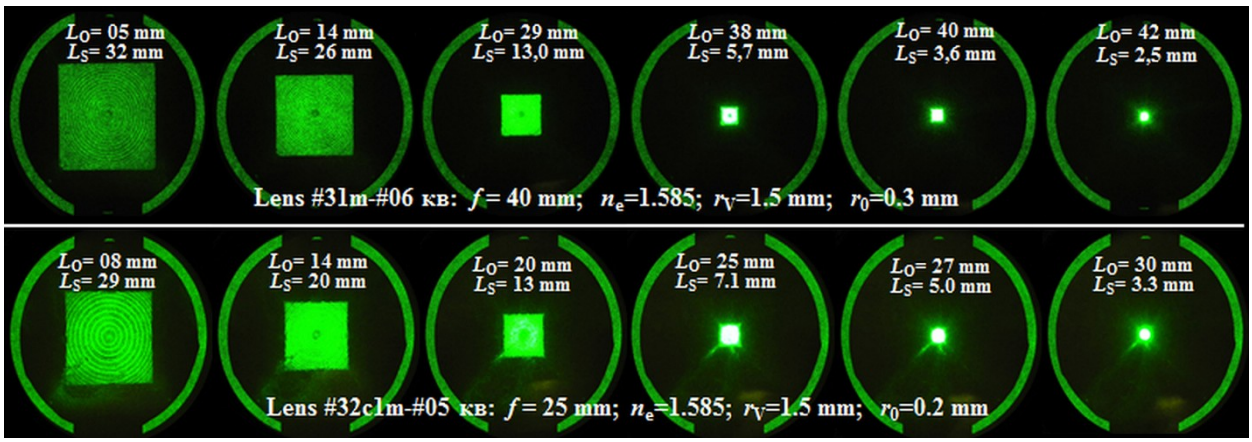

Fig. 14. Screen images of the lenses #31m-#06 and #32c1m-#05, diaphragmed to the size of 35×35 mm^2, depending on the observation distance L_0.

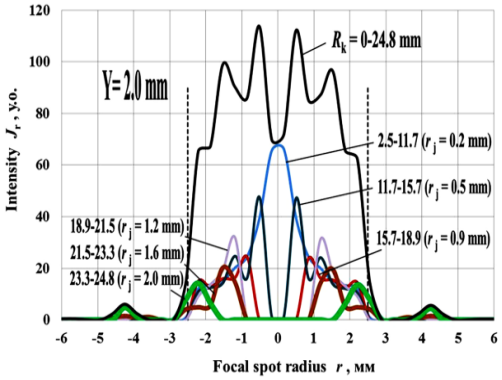

(a)

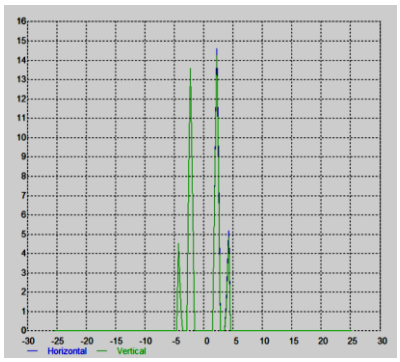

(b)

Fig. 15. Modeled focal image profiles for the lens #32c1: a) light distribution over different lens zones, b) profile for the zones #13–15 (R_k = 23.3…24.8) with an additional maximum at r_V = 4.3 mm.

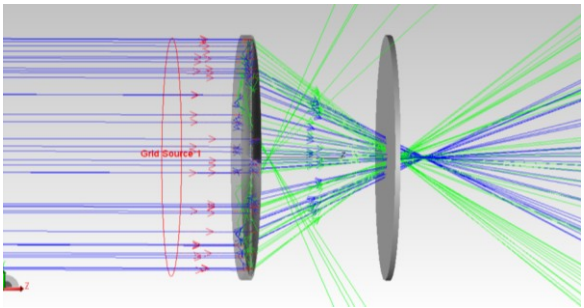

Fig. 16. Simulated rays path for the zones #13–15 of the lens #32-c1.

The incident "red" rays with an intensity of 66 to 100%, after being refracted by the lens zones # 13-15, are transformed into the "green" rays (the intensity of 33–66%), because the refraction angles for these zones α_k = 38.211…38.437 deg. are approaching the critical value α_k = 39.118 deg. and the light transmission coefficients are τ^S_k = 0.607…0.541. These rays form the main maxima in the center of the focal plane. At the same time, the blue rays also appear (the intensity of 0–33%) due to the multiple Fresnel reflections of the rays inside the lens. These rays form additional maxima in the focal zone of r_V=4.3 mm. Its intensity is ~ 30% of the main maxima (see Fig. 15b). Similarly, the prism zones # 11-12 with R_k=21.5…23.3 mm also form an additional maximum with the intensity of 8.3% at the same radius r_V=4.3 mm. Other lens zones with lower radii R_k<21.5 mm and angles α_k<36.22 deg. according to computer modeling revealed only the main maxima (see Fig. 15a), which are placed for radii r_j=0.2, 0.5, 0.9, and 1.2 mm, respectively, set during the simulation.

Therefore, when using such a lens for illuminating solar modules, it is advisable to diaphragm it and to use only prismatic zones with radii R_k<21.5 mm. All the light profiles shown in Fig. 15 are computer simulated. In reality, the total laser profiles for the lens #32-c1 are smoother due to the light beam scattering at the relief defects (see Figs. 10 and 11).

Another option to reduce the light profile extension is to create a similar "solar" lens, but with a larger focal length f_0=40…50 mm, at which the refraction angles of the microprisms do not exceed the value $\alpha_k \approx$34.0 deg. This diminishes the negative internal reflection and increases the total light transmission coefficient of the lenses to the values τ^S_k=82–85% [19, 20].

Therefore, in further creation of plane-focusing lenses for concentrator solar energy modules based on crystalline silicon, it is advisable to use a focusing optimization scheme with a central "dark" area with a radius r_j=0.2…0.3 mm and an image size r_V=1.5…2.5 mm. The optimal focal length of the lenses is f_0=40…50 mm. It is also advisable to diaphragm the light flux by forming square lenses to reduce flux losses. The exact size of the illuminated zone of a photodetector can be adjusted by respectively changing the focusing distance of the lenses.

4. Conclusions

Lens designs were proposed, geometric parameters were calculated, and experimental samples of specialized plane-focusing light concentrators were manufactured from optical polycarbonate by diamond microcutting for concentrator solar energy systems.

Metal stamp-matrices were created and formed using the diamond microcutting technique for replicating the required number of plane-focusing lenses by the thermopressing method.

Using collimated laser beam, photo-technical characteristics of the test samples of focusing elements were experimentally investigated. The obtained results showed the correspondence of experimental data to the calculated characteristics.

Square-shaped diaphragm lenses were created to match the shape of the light flux with square solar cells, and the photo-technical characteristics of their test samples were experimentally determined. It was shown that such lenses create homogeneous illumination of the surface in the form of a square with the dimensions of 5.0×5.0 mm^2 required for the solar cell that are planned for the future researches.

References

1. Chen Y., Pu S., Hou M. *et al.* Lightweight and efficient beam-shaping metalens for converting Gaussian beams into 2D flat-top beams. *Opt. Express*. 2025. **33**, No 5. P. 11555–11573. P. 555456. https://doi.org/10.1364/OE.555456.

2. Tan N., Jin Y., Neo D.W.K. *et al.* Ultra-precision direct diamond shaping of functional micro features. *J. Manuf. Process*. 2021. **64**. P. 209–223. https://doi.org/10.1016/j.jmapro.2020.12.064.
3. Tan N., Jin Y., Lim Z. *et al.* Design and fabrication of composite polygonal Fresnel lenses. *Opt. Exp*. 2021. **29**. P.36516–36534. https://doi.org/10.1364/OE.436290
4. Geints Y.E., Panina E.K., Minin I.V., Minin O.V. Study of focusing parameters of wavelength-scale binary phase Fresnel zone plate. *J. Opt*. 2021. **23**. P. 065101. https://doi.org/10.1088/2040-8986/abf891.
5. Kuang Z., Lee J., Edwardson S. *et al.* Ultrafast laser beam shaping for material processing at imaging plane by geometric masks using a spatial light modulator. *Opt. Lasers Eng*. 2015. **70**. P. 1–5. https://doi.org/10.1016/j.optlaseng.2015.02.004.
6. Häfner T., Strauß J., Roider C. *et al.* Tailored laser beam shaping for efficient and accurate micro-structuring. *Appl. Phys. A*. 2018. **124**, No 111. P. 1–9. https://doi.org/10.1007/s00339-017-1530-0.
7. Le H., Penchev P., Henrottin A. *et al.* Effects of top-hat laser beam processing and scanning strategies in laser micro-structuring. *Micromachines*. 2020. **11**, No 2. P. 221. https://doi.org/10.3390/mi11020221.
8. Ma H., Liu Z., Jiang P. *et al.* Improvement of Galilean refractive beam shaping system for accurately generating near-diffraction-limited flattop beam with arbitrary beam size. *Opt. Express*. 2011. **19**. P. 13105–13117. https://doi.org/10.1364/OE.19.013105.
9. Wu J., Zhang H., Zhang W. *et al.* Single-shot lensless imaging with Fresnel zone aperture and incoherent illumination. *Light Sci. Appl.* 2020. **9**, No 53. https://doi.org/10.1038/s41377-020-0289-9.
10. Bachhav C.Y., Sonawwanay P.D. Study on design and performance enhancement of Fresnel lens solar concentrator. *Mater. Today. Proc*. 2022. **56**. P. 2873–2879. https://doi.org/10.1016/j.matpr.2021.10.168.
11. Montanet E., Rodat S., Falcoz Q., Roget F. Influence of topography on the optical performances of a Fresnel linear asymmetrical concentrator array: The case of the ELLO solar power plant. *Energy*. 2023. **274**. P. 127310. http://doi.org/10.1016/j.energy.2023.127310.
12. Antonov E.E., Fu M.L., Petrov V.V. *et al.* Structure of microprismatic fresnel lenses for creating uniform focal images. *Opt. Express.* 2021. **29**, No 24. P. 38958–38970. https://doi.org/10.1364/OE.438590.
13. Fu M.L., Antonov E.E., Lysenko V.S. *et al.* Uniform illumination of concentrated sunlight in photovoltaic solar modules with plane-focusing Fresnel lenses. *IEEE Photon. J*. 2023. **15**, No 4. P. 5000310. https://doi.org/10.1109/JPHOT.2023.3288155.
14. Ju X., Pan X., Zhang Z. *et al.* Thermal and electrical performance of the dense-array concentrating photovoltaic (DA-CPV) system under nonuniform illumination. *Appl. Energy*. 2019. **250-c**. P. 904–915. https://doi.org/10.1016/j.apenergy.2019.05.083.
15. Xie W.T., Dai Y.I., Wang R.Z., Sumathy K. Concentrated solar energy applications using Fresnel lenses: A review. *Renew. Sustain. Energy Rev*. 2011. **15**. P. 2588–2606. https://doi.org/10.1016/j.rser.2011.03.031.
16. Yamada N., Okamoto K. Experimental measurements of a prototype high concentration Fresnel lens CPV module for the harvesting of diffuse solar radiation. *Opt. Express.* 2014. **22**, No 101. P. A28–A34. https://doi.org/10.1364/OE.22.00A28.
17. Sachenko A., Kostylyov V., Sokolovskyi I., Evstigneev M. Effect of temperature on limit photoconversion efficiency in silicon solar cells. *IEEE J. Photovolt*. 2020. **10**, No 1. P. 63–69. https://doi.org/10.1109/JPHOTOV.2019.2949418.
18. Brinksmeier E., Glabe R., Schonemann L. Diamond micro chiseling of large-scale retroreflective arrays. *Prec. Eng*. 2012. **36**. P. 650–657. https://doi.org/10.1016/j.precisioneng.2012.06.001.
19. Petrov V., Kryuchyn A., Antonov E. *et al.* Optical phenomena in microprism diagnostic set KK-42. *Proc. SPIE*. 2011. **8011**, 22nd Congress of the International Commission for Optics: Light for the Development of the World. P. 80119A. https://doi.org/10.1117/12.900751.
20. Fu M.L., Antonov E., Manko D. *et al.* Achromatic refractive-diffractive double-relief microprisms. *Opt. Laser Eng*. 2020. **126**. P. 105903. https://doi.org/10.1016/j.optlaseng.2019.105903.
21. Jmage J Program. https://soft.mydiv.net/win/download-ImageJ.html
22. Sultanova N., Kasarova S., Nikolov I. Dispersion properties of optical polymers. *Acta Phys. Pol. A*. 2009. **116**. P. 585–587. https://doi.org/10.12693/APhysPolA.116.585.
23. Gorban A.P., Kostylyov V.P., Sachenko A.V., Serba A.A. The efficiency limit for diffusion silicon solar cells at concentrated illumination. *SPQEO*. 1999. **2**. P. 45–49. https://doi.org/10.15407/spqeo2.02.045.
24. Korkishko R., Vlasiuk V., Kostylyov V. *et al.* Optimization of silicon solar cell design for use under concentrated solar irradiation. *Technology and Design in Electronic Equipment*. 2024. **1-2**. P. 3–10. https://doi.org/10.15222/tkea2024.1-2.03.
25. Sachenko A.V., Gorban A.P., Kostylyov V.P. *et al.* Comparative analysis of photoconversion efficiency in the Si solar cells under concentrated illumination for the standard and rear geometries of arrangement of contacts. *Semiconductors.* 2007. **41**. P. 1214–1223. https://doi.org/10.1134/S106378260710017X.
26. Sachenko A., Kostylyov V., Korkishko R. *et al.* Simulation and characterization of planar high-efficiency back contact silicon solar cells. *SPQEO*. 2021. **24**. P. 319–327. https://doi.org/10.15407/spqeo24.03.319.
27. Cotal H., Fetzer C., Boisvert J. *et al.* III–V multijunction solar cells for concentrating photovoltaics. *Energy Environ. Sci*. 2009. **2**. P. 174–192. https://doi.org/10.1039/b809257e.
28. Baig H., Heasman K.C., Mallick T.K. Non-uniform illumination in concentrating solar cells. *Renew. Sustain. Energy Rev.* 2012. **12**. P. 5890–5909. http://doi.org/10.1016/j.rser.2012.06.020.
29. SOLIDWORKS 2020. http://www.solidworks.com.
30. Software for design and analysis of illumination and optical systems: https://www.lambdares.com/tracepro/

Appendix A

Simulation of Fresnel lens rV = 2,5 мм with r_i = 0.2 (4 zones) - 0.5 (2 zones)- 0.9 (2 zones) - 1.2 (2 zones) - 1.6 (2 zones) - 2.0 (3 zones) mm

f = 25 mm, λ=0.585 μm (n_1 = 1.585); δ= 6.0 mm, $\alpha_{k\,max}$ = 39.118 deg., τ^R(Fr1) = 0.949; τ^R (Fr2) = 0.901. τ^V_k= 1/ (1+ tgα$_k$ tgθ) # 32-c1

$\Delta R'_k = W_j \operatorname{tg}\alpha_k \operatorname{tg}\gamma_k / (1 - \operatorname{tg}\alpha_k \operatorname{tg}\gamma_k)$ $\Delta R^{\theta}_k = \Delta R_k \cos\theta + (h_k - h_{k-1}) \sin\theta$ $h_k = W_j \operatorname{tg}\alpha_k \{1 + \operatorname{tg}\alpha_k \operatorname{tg}\gamma_k / (1 - \operatorname{tg}\alpha \operatorname{tg}\gamma)\}$

Lens with reverse angle θ = 0 deg.

n	n			range	R_k=R_0+ΔR_k	γ_k=tg^{-1}(R_k/f)		α_k= tg^{-1}{sinγ/(1,585–cosγ$_k$)}			ΔR_k = h_k/ tgα$_k$	ΔL_k=ΔR_k/cosα$_k$	β=90–α	h_k	γ+α
	zone	r_i	R_k, mm	mm	R_0= 2,0 mm	rad.	deg.	rad.	deg.	deg.	mm	mm		μm	deg.
				2,500 - 0,000	0.000000	0.000000	0.00								
	1	0.20	4.800000	4,800 - 2,500	2.500000	0.091742	5.26	0.154251	8.837917	0.000	1.15000	1.16	90.000	0.000	5.26
1		0.20			3.650000	0.091742	5.26	0.154251	8.837917	8.838	1.15000	1.16	81.162	178.809	14.09
2	2	0.20	7.100000	7,100 - 4,800	4.800000	0.181965	10.43	0.292233	16.743731	8.838	0.76667	0.80	81.162	178.809	19.26
3		0.20			5.566667	0.181965	10.43	0.292233	16.743731	16.744	0.76667	0.80	73.256	230.649	27.17
4		0.20			6.333333	0.181965	10.43	0.292233	16.743731	16.744	0.76667	0.80	73.256	230.649	27.17
5	3	0.20	9.400000	9,400 - 7,100	7.100000	0.269296	15.43	0.404745	23.190166	16.744	0.76667	0.83	73.256	230.649	32.17
6		0.20			7.866667	0.269296	15.43	0.404745	23.190166	23.190	0.76667	0.83	66.810	328.438	38.62
7		0.20			8.633333	0.269296	15.43	0.404745	23.190166	23.190	0.76667	0.83	66.810	328.438	38.62
8	4	0.20	11.700000	11,700 - 9,400	9.400000	0.352620	20.20	0.490610	28.109874	23.190	0.57500	0.65	66.810	328.438	43.39
9		0.20			9.975000	0.352620	20.20	0.490610	28.109874	28.110	0.57500	0.65	61.890	307.149	48.31
10		0.20			10.550000	0.352620	20.20	0.490610	28.109874	28.110	0.57500	0.65	61.890	307.149	48.31
11		0.20			11.125000	0.352620	20.20	0.490610	28.109874	28.110	0.57500	0.65	61.890	307.149	48.31
12	5	0.50	13.700000	13,700 - 11,700	11.700000	0.421189	24.13	0.546313	31.301409	28.110	0.50000	0.59	61.890	307.149	52.24
13		0.50			12.200000	0.421189	24.13	0.546313	31.301409	31.301	0.50000	0.59	58.699	304.022	55.43
14		0.50			12.700000	0.421189	24.13	0.546313	31.301409	31.301	0.50000	0.59	58.699	304.022	55.43
15		0.50			13.200000	0.421189	24.13	0.546313	31.301409	31.301	0.50000	0.59	58.699	304.022	55.43
16	6	0.50	15.700000	15,700 - 13,700	13.700000	0.485796	27.83	0.587787	33.677690	31.301	0.50000	0.60	58.699	304.022	59.14
17		0.50			14.200000	0.485796	27.83	0.587787	33.677690	33.678	0.50000	0.60	56.322	333.177	61.51
18		0.50			14.700000	0.485796	27.83	0.587787	33.677690	33.678	0.50000	0.60	56.322	333.177	61.51
19		0.50			15.200000	0.485796	27.83	0.587787	33.677690	33.678	0.50000	0.60	56.322	333.177	61.51
20	7	0.90	17.300000	17,300 - 15,700	15.700000	0.534516	30.63	0.612840	35.113149	33.678	0.40000	0.49	56.322	333.177	64.30
21		0.90			16.100000	0.534516	30.63	0.612840	35.113149	35.113	0.40000	0.49	54.887	281.262	65.74
22		0.90			16.500000	0.534516	30.63	0.612840	35.113149	35.113	0.40000	0.49	54.887	281.262	65.74
23		0.90			16.900000	0.534516	30.63	0.612840	35.113149	35.113	0.40000	0.49	54.887	281.262	65.74
24	8	0.90	18.900000	18,900 - 17,300	17.300000	0.580582	33.26	0.632183	36.221439	35.113	0.40000	0.50	54.887	281.262	68.38
25		0.90			17.700000	0.580582	33.26	0.632183	36.221439	36.221	0.40000	0.50	53.779	292.986	69.49
26		0.90			18.100000	0.580582	33.26	0.632183	36.221439	36.221	0.40000	0.50	53.779	292.986	69.49
27		0.90			18.500000	0.580582	33.26	0.632183	36.221439	36.221	0.40000	0.50	53.779	292.986	69.49
28	9	1.20	20.200000	20,200 - 18,900	18.900000	0.616075	35.30	0.644500	36.927123	36.221	0.43333	0.54	53.779	292.986	71.52
29		1.20			19.333333	0.616075	35.30	0.644500	36.927123	36.927	0.43333	0.54	53.073	325.677	72.23
31		1.20			19.766667	0.616075	35.30	0.644500	36.927123	36.927	0.43333	0.54	53.073	325.677	72.23
32	10	1.20	21.500000	21,500 - 20,200	20.200000	0.649870	37.23	0.654328	37.490249	36.927	0.43333	0.55	53.073	325.677	74.16
33		1.20			20.633333	0.649870	37.23	0.654328	37.490249	37.490	0.43333	0.55	52.510	332.391	74.73
34		1.20			21.066667	0.649870	37.23	0.654328	37.490249	37.490	0.43333	0.55	52.510	332.391	74.73
35	11	1.60	22.400000	22,400 - 21,500	21.500000	0.672297	38.52	0.659905	37.809768	37.490	0.30000	0.38	52.510	332.391	76.01
36		1.60			21.800000	0.672297	38.52	0.659905	37.809768	37.810	0.30000	0.38	52.190	232.786	76.33
37		1.60			22.100000	0.672297	38.52	0.659905	37.809768	37.810	0.30000	0.38	52.190	232.786	76.33
38	12	1.60	23.300000	23,300 - 22,400	22.400000	0.693951	39.76	0.664620	38.079914	37.810	0.30000	0.38	52.190	232.786	77.57
39		1.60			22.700000	0.693951	39.76	0.664620	38.079914	38.080	0.30000	0.38	51.920	235.063	77.84
40		1.60			23.000000	0.693951	39.76	0.664620	38.079914	38.080	0.30000	0.38	51.920	235.063	77.84
41	13	2.00	23.800000	23,800 - 23,300	23.300000	0.705654	40.43	0.666907	38.210966	38.080	0.16667	0.21	51.920	235.063	78.51
42		2.00			23.466667	0.705654	40.43	0.666907	38.210966	38.211	0.16667	0.21	51.789	131.205	78.64
43		2.00			23.633333	0.705654	40.43	0.666907	38.210966	38.211	0.16667	0.21	51.789	131.205	78.64
44	14	2.00	24.300000	24,300 - 23,800	23.800000	0.717128	41.09	0.668979	38.329651	38.211	0.16667	0.21	51.789	131.205	79.30
45		2.00			23.966667	0.717128	41.09	0.668979	38.329651	38.330	0.16667	0.21	51.670	131.766	79.42
46		2.00			24.133334	0.717128	41.09	0.668979	38.329651	38.330	0.16667	0.21	51.670	131.766	79.42
47	15	2.00	24.800000	24,800 - 24,300	24.300000	0.728378	41.73	0.670850	38.436858	38.330	0.16667	0.21	51.670	131.766	80.06
48		2.00			24.466667	0.728378	41.73	0.670850	38.436858	38.437	0.16667	0.21	51.563	132.273	80.17
49		2.00			24.633334	0.728378	41.73	0.670850	38.436858	38.437	0.16667	0.21	51.563	132.273	80.17
50		2.00		25.300	24.800000	0.739406	42.36	0.672535	38.533413	38.437	0.50000	0.64	51.563	132.273	80.80
					25.300000										

Authors' contributions

Antonov E.E.: conceptualization, formal analysis, investigation, validation, visualization, writing – original draft.

Chernenko V.V.: conceptualization, formal analysis, validation, writing – review & editing.

Kostylyov V.P.: conceptualization, formal analysis, validation, writing – review & editing.

Lysenko V.S.: conceptualization, methodology, formal analysis, supervision, writing – review & editing.

Manko D.Yu.: investigation, validation, visualization, writing – review & editing.

Martynyuk I.A.: investigation, validation, software and hardware.

Petrov V.V.: investigation, project administration, supervision, writing – review & editing.

Zenin V.N.: investigation, validation, software and hardware.

Authors and CV

Eugene Antonov, Doctor of Engineering Sciences, Leading Researcher of the Institute for Information Recording NAS of Ukraine. Now he specializes in optical properties of microprisms. He is the author of more than 140 scientific works, including 2 monographs and 13 patents. http://orcid/0000-0003-4471-8287

Volodymyr Chernenko, PhD, Senior Researcher at the V. Lashkaryov Institute of Semiconductor Physics NAS of Ukraine. He is the author of more than 100 scientific publications. His main research interests include research and analysis of silicon solar cells. E-mail: vvch@isp.kiev.ua, https://orcid.org/000-002/7630/6925

Vitaliy Kostylyov, Professor, Doctor of Sciences in Physics and Mathematics, Head of the PV Converters and PV Panels Testing Center, V. Lashkaryov Institute of Semiconductor Physics NAS of Ukraine. Authored over 300 scientific publications. Research interests: photovoltaics and betavoltaics, research, analysis and modelling of solar cells, testing solar cells.
https://orcid.org/0000-0002-1800-9471

Volodymyr Lysenko, Professor, Doctor of Sciences in Physics and Mathematics, Corresponding Member of the NAS of Ukraine since 1992, Chief Researcher of the V. Lashkaryov Institute of Semiconductor Physics NAS of Ukraine. His research areas are micro-, nano- and optoelectronics, information technologies, and nanoparticles for antiviral and anticancer therapy. He is the author of 5 monographs and more than 350 scientific works.
E-mail: lysenko.v@nas.gov.ua,
http://orcid.org/ 0000-0001-9948-9499

Dmytro Manko, PhD, Researcher. He is the author of more than 70 scientific works, including 3 monographs and more than 10 patents. His research interests are computer science, applied optics, and light polarization.
E-mail: dmitriy.manko@gmail.com,
http://orcid.org/0000-0003-1848-2952

Ivan Martynyuk graduated from the Kiev Polytechnic Institute, worked at state energy enterprises for many years, specialist in electro-technical field. Now he is conducting precise experiments in pneumatic pressing and hydraulic thermopressing technology, constructing appropriate control and measuring instruments for manufacturing final microprismatic products from optical plastics.

Viacheslav Petrov, Doctor of Sciences, Professor, Academician of the NAS of Ukraine since 2012. Prof. Petrov is the Director of the Institute for Information Recording NAS of Ukraine. Research interests: long-term storage of digital information, microprisms for ophthalmology applications, scientometrics, and applied optics. He is the author of more than 600 scientific works, including 8 monographs and more than 230 patents. He is awarded by 16 Ukrainian and international awards.
E-mail: petrov@ipri.kiev.ua,
http://orcid.org/0000-0002-7265-9889

Volodymyr Zenin graduated from the Kyiv Polytechnic Institute. He is the Researcher of the Institute for Information Recording NAS of Ukraine. He has carried out a series of works on development of technological equipment for implementation of diamond microcutting method, investigated optical properties of retroreflective devices and homogenizer for optical radiation. Authored over 40 scientific works and patents. E-mail: zen51vlad@gmail.com

Плоско-фокусувальна оптика для кремнієвих сонячних фотоперетворювачів

Е.Е. Антонов, В.В. Черненко, В.П. Костильов, В.С. Лисенко, Д.Ю. Манько, І.О. Мартинюк, В.В. Петров, В.Н. Зенін

Анотація. Розроблено алгоритм моделювання та розраховано геометричні параметри плоско-фокусувальних лінз для концентраторних сонячних систем з кремнієвими фотоперетворювачами. Такі лінзи формують гомогенне зображення у фокальній площині, тому вони є перспективними для використання в таких системах та дозволяють мінімізувати теплові та електричні втрати в сонячних модулях, пов'язані з неоднорідним освітленням поверхні фотоперетворювача. Розроблено відповідну технологію виготовлення штамп-матриць методом алмазного мікроточіння. На основі результатів моделювання сформовано деякі зразки плоско-фокусувальних лінз методом термопресування з використанням металевих матриць. Виготовлені зразки спеціалізованих трансформуючих мікропризматичних структур квадратної форми було експериментально досліджено за допомогою колімованого лазерного променя.

Ключові слова: алгоритм моделювання мікропризм, плоско-фокусувальна оптика, мікрорельєфна структура.